Original Article

Investigation of urinary components in rat model of ketamine-induced bladder fibrosis based on metabolomics

Haozhen Li[1]^, Quan Zhu[1], Kaixuan Li[1], Ziqiang Wu[1], Zhengyan Tang[1,2], Zhao Wang[1]^

[1]Department of Urology, Xiangya Hospital, Central South University, Changsha, China; [2]Hunan Provincial Engineering Laboratory for Diagnosis and Treatment of Genitourinary System Disease, Changsha, China

Contributions: (I) Conception and design: Z Wang, Z Tang, H Li; (II) Administrative support: Z Wang, Z Tang; (III) Provision of study materials or patients: None; (IV) Collection and assembly of data: H Li, Q Zhu, K Li; (V) Data analysis and interpretation: H Li, Z Wang; (VI) Manuscript writing: All authors; (VII) Final approval of manuscript: All authors.

Correspondence to: Zhengyan Tang. Department of Urology, Xiangya Hospital, Central South University, Changsha 410008, China; Hunan Provincial Engineering Laboratory for Diagnosis and Treatment of Genitourinary System Disease, Changsha 410008, China. Email: xytzyan@163.com; Zhao Wang. Department of Urology, Xiangya Hospital, Central South University, Changsha 410008, China. Email: xywangz07@163.com.

Background: Ketamine abuse has been linked to the system's damage, presenting with lower urinary tract symptoms (LUTS). While the pathogenesis of ketamine-induced urinary damage is not fully understood, fibrosis is believed to be a potential mechanism. A metabolomic investigation of the urinary metabolites in ketamine abuse was conducted to gain insights into its pathogenesis.

Methods: A rat model of ketamine induced bladder fibrosis was established through tail vein injection of ketamine hydrochloride and control group was established through tail vein injection of the equivalent normal saline. Hematoxylin and eosin (H&E) staining and Masson trichrome staining were performed to evaluated bladder pathology. Urinary components were detected based on a metabolomic approach using ultra-high performance liquid tandem chromatography quadrupole time of flight mass spectrometry (UHPLC-QTOFMS platform). Orthogonal projections analyzed the data to latent structures discriminant analysis (OPLS-DA) and bioinformatics analysis.

Results: The rat model of ketamine induced bladder fibrosis was confirmed through H&E and Masson trichrome staining. There were marked differences in the urinary metabolites between the experimental group and the control group. Compared to the control group, 16 kinds of differential metabolites were up-regulated and 102 differential metabolites were down-regulated in the urine samples of the ketamine group. Bioinformatics analysis revealed the related metabolic pathways.

Conclusions: Using a ketamine-induced bladder fibrosis rat model, this study identified the differential urinary metabolites expressed following ketamine treatment. These results provide vital clues for exploring the pathogenesis of ketamine-induced LUTS and may further contribute to the disease's diagnosis and treatment.

Keywords: Ketamine; bladder fibrosis; metabolomics

Submitted Aug 26, 2020. Accepted for publication Dec 21, 2020.
doi: 10.21037/tau-20-1202
View this article at: http://dx.doi.org/10.21037/tau-20-1202

^ ORCID: Haozhen Li, 0000-0003-0859-1960; Zhao Wang, 0000-0003-1980-2866.

Introduction

Ketamine is a derivative of phencyclidine and has been used as an anesthetic in clinical practice since the 1960s (1). It was found to have hallucinogenic and psychoactive effects on ketamine abusers (2). In 2007, Shahani *et al.* were the first to report the lower urinary tract symptoms (LUTS) caused by ketamine abuse. The symptoms included severe dysuria, frequency, urgency, and gross hematuria (3). Severe clinical cases can present with thickening of the bladder wall and bladder contracture. In emergency cases, hydronephrosis, uremia, and other serious complications have also been reported (4-6). Life quality would be seriously affected by refractory LUTS, and the abusers may even encounter life-threatening situation (7). Some pathological studies have revealed bladder fibrosis in the ketamine abusers. Also, animals injected with ketamine can generate ketamine associated cystitis model (8-10). However, the pathogenesis of ketamine-induced LUTS is not fully understood. Furthermore, treatment regimens are limited, especially in patients with serious bladder contracture and renal insufficiencies. Therefore, it is essential to elucidate the mechanisms of ketamine-associated bladder fibrosis to improve chronic ketamine abusers' prognosis.

Pathological studies have demonstrated urothelial ulceration, erosion, tearing and infiltration of inflammatory cells in the bladder of patients with ketamine-associated LUTS (11). Several investigations have suggested that the direct or indirect effects of ketamine and its urinary metabolites may be important in the pathogenesis of bladder inflammation, fibrosis, subsequent lesions (7,11). Therefore, this study examined the differential metabolites in the urine samples of rats with ketamine-induced bladder fibrosis. This will provide important insights into the pathogenesis of bladder fibrosis and facilitate its early detection by assessing the differential metabolites' levels.

Metabolomics is an important branch of systems biology to identify different metabolite expression via high-throughput methods (12). Metabolomics is divided into non-targeted metabolomics and targeted metabolomics. The former of which enables extensive screening of metabolites (13). High throughput detection of metabolomics can efficiently accomplish the qualitative and quantitative analyses of metabolites, and can further recognize the differential expression of metabolites in various groups. Identification of the differential metabolites will contribute to understanding the pathogenesis of ketamine-associated LUTS and may be applied to the disease's diagnosis.

In this study, we established a rat model of ketamine induced bladder fibrosis. After confirming the fibrosis of bladder, we detect the differential urine metabolites and associated pathways based on metabolomics.

We present the following article in accordance with the ARRIVE reporting checklist (available at http://dx.doi.org/10.21037/tau-20-1202).

Methods

Rat model and the collection of urine samples

Experiments were performed under a project license (No. 2018sydw0225) granted by experimental animal welfare center in Central South University, Hunan, China, in compliance with China's "Animal management regulations" for the care and use of animals.

Female 8-week-old Sprague-Dawley (SD) rats (200–250 g) were purchased from Hunan Slack Jingda Experimental Animal Corporation (Hunan, China). The rats were housed in a specific pathogen-free (SPF) environment at room temperature (20–26 ℃) in 40–70% humidity under a 12-hour/12-hour light/dark cycle, and given free access to food and water.

To establish a rat model of ketamine-induced bladder fibrosis, 20 SD rats were randomly divided into two groups, with 10 rats in each group. In the control group, 2 mL normal saline was injected daily into the animals' tail vein. In the experimental group, a 0.1 g/2 mL ketamine hydrochloride solution (Fujian Gutian Pharmaceutical Co. Ltd.) was injected daily into each rat's tail vein. After 8 weeks of injections, urine was collected every morning for the first 2 hours for 3 consecutive days. After collection, the urine samples were transferred to frozen tubes for centrifugation (4 ℃, 10,000 rpm, 10 min) and placed in liquid nitrogen for cryopreservation before analysis. The rats were anesthetized by pentobarbital injection (2%, 40 mg/kg) and sacrificed by cervical dislocation. After adequate perfusion of systemic tissues through cardiac infusion with 4% paraformaldehyde, bladder tissues were immediately removed and transferred to 4% paraformaldehyde for fixation.

Histopathological observation

Hematoxylin and eosin (HE) staining and Masson trichrome staining were performed to examine the bladder tissue histopathology. After 24 hours of fixation in 4% paraformaldehyde, bladder tissues were embedded in

wax blocks. Following this, 4 μm sections were dewaxed, rehydrated, and stained. A standard HE and Masson trichrome staining procedure was performed according to previous protocols (14,15).

Differential metabolomics detection

For differential metabolomic analyses, 100 μL of urine sample was mixed with 400 μL extract solution (acetonitrile:methanol =1:1) containing an internal standard (L-2-chlorophenylalanine, 2 μg/mL). The samples were sonicated for 10 min in ice-water bath after 60 s vortex. Then the samples were incubated at –40 ℃ for 1 hour and centrifuged at 10,000 rpm at 4 ℃ for 15 min. The samples were mixed with 200 μL of 50% acetonitrile after drying, sonicated on ice for ice and centrifuged at 13,000 rpm for 15 min at 4 ℃. Furthermore, 10 μL of each sample were mixed to be the quality control (QC) sample.

The Agilent 1290 Infinity series ultra-high performance liquid chromatography (UHPLC) System (Agilent Technologies) works with UPLC BEH Amide column (2.1×100 mm, 1.7 μm). The mobile phase A consisted of ammonium acetate and ammonia hydroxide. The mobile phase B consisted of acetonitrile. Elution gradient conditions were as follows: 0–0.5 min, 95% B; 0.5–7.0 min, 95–65% B; 7.0–8.0 min, 65–40% B; 8.0–9.0 min, 40% B; 9.0–9.1 min, 40–95% B; 9.1–12.0 min, 95% B. The auto-sampler temperature was 4 ℃. The column temperature was 25 ℃ and the injection volume was 1 μL (positive) or 1 μL (negative).

Data analysis

The mass spectrometry (MS) raw data (.wiff) files were converted to the mzXML format by ProteoWizard, and processed by R package XCMS (version 3.2). The procedure consisted of peak deconvolution, alignment and integration. The Minfrac index was 0.5 and the cut-off index was 0.6. MS2 database in-house was applied for the identification of metabolites. The Kyoto Encyclopedia of Genes and Genomes (KEGG, www.kegg.jp) online database was used to explore the metabolic pathways and function.

Statistical analysis

The experimental data were analyzed by SPSS statistical software (version 20.0). The measurement data were expressed as mean ± standard deviation and there are 10 biological replications in each group. Data were statistically analyzed at P value less than 0.05.

Results

Hematoxylin and eosin staining and Masson trichrome staining of bladder tissue

After consecutive 8 weeks intravenous injection of ketamine, bladder specimens were analyzed through HE and Masson trichrome staining. Representative bladder tissue sections are presented in *Figure 1*. Compared to the control group (*Figure 1A*), the bladder specimens in the ketamine-treated group showed that the urothelium was denuded, accompanied by vascular congestion and inflammatory cell infiltration (*Figure 1B*). Bladder fibrosis was also confirmed through Masson trichrome staining (*Figure 1D*). Extracellular matrix (ECM) and collagen deposition were obvious in the ketamine treated group compared to the control group.

Orthogonal projections to latent structures-discriminant analysis (OPLS-DA)

In order to visualize and further analysis the data, the results were examined using the OPLS-DA test. Orthogonal variables that were not related to the categorical variables were filtered out. to obtain more reliable group differences for the metabolites (*Figure 2*). The results indicated that all of the samples in both groups were in the 95% confidence interval.

The OPLS-DA permutation test was used to evaluate the model's validity using the R^2Y (model interpretability of categorical variable Y) and Q^2 (model predictability) values obtained after cross-validation. In addition, different random Q^2 values were obtained by indiscriminately changing the order of the categorical variable Y several times (*Figure 2*). The results showed that the established model was consistent with the real sample data. Further analysis revealed that the original model demonstrated good robustness without any evidence of overfitting.

Expression of differential metabolites

The detected differential metabolites were further screened though statistical analysis. The criteria were as following: Student's *t*-test P value less than 0.05, and variable importance in the projection (VIP) value of OPLS-DA model was greater

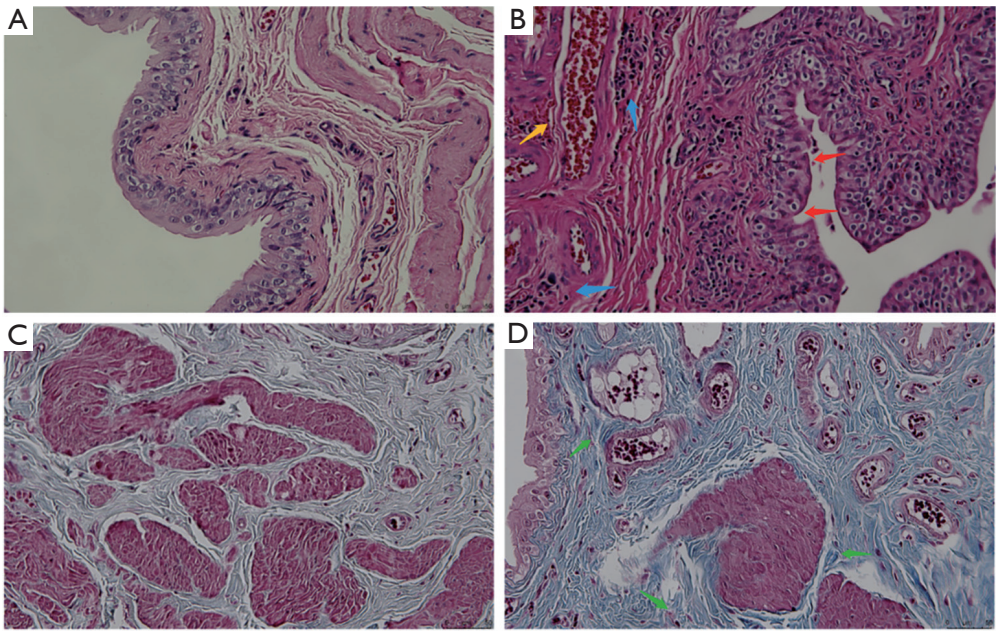

Figure 1 Histopathological changes of bladder specimen induced by 8-week ketamine injection in rat. Comparison between the control group (A) and ketamine group (B) through HE staining showed urothelium desquamation (red arrow), inflammatory cell infiltration (blue arrow), vascular distension and congestion (yellow arrow) in ketamine group. Bladder fibrosis was confirmed via Masson trichrome staining in control (C) and ketamine group (D). It showed collagen deposition (green arrow). Original magnification ×100.

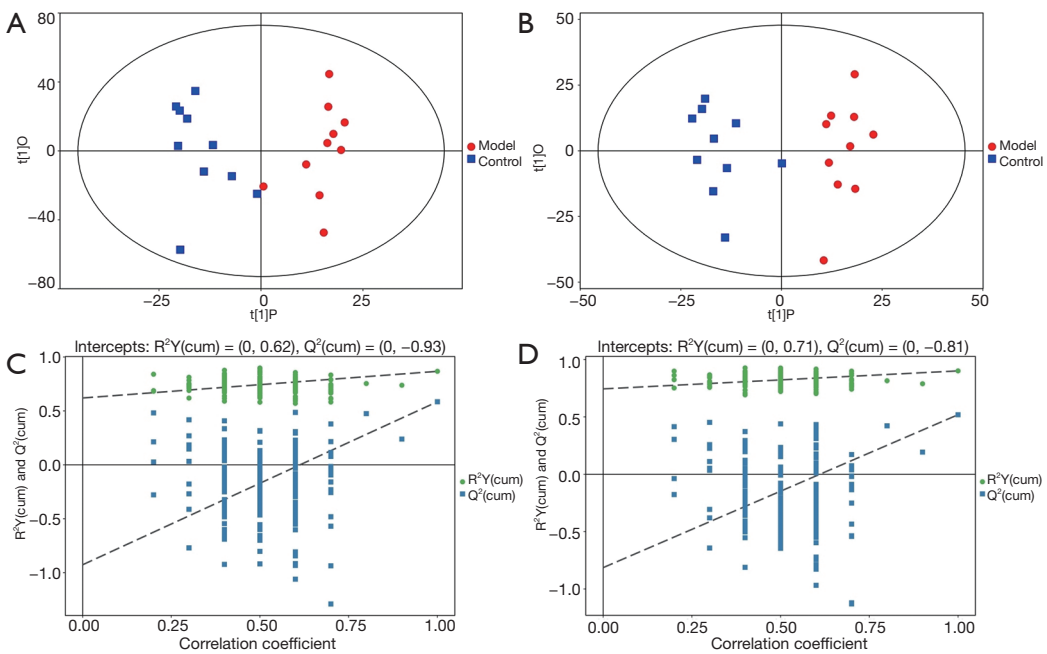

Figure 2 Score scatter plot of OPLS-DA model for ketamine group vs. control group (A for negative ion and B for positive ion mode) and permutation test of OPLS-DA model for ketamine group *vs.* control group (C for negative ion and D for positive ion mode). OPLS-DA, orthogonal projections to latent structures-discriminant analysis.

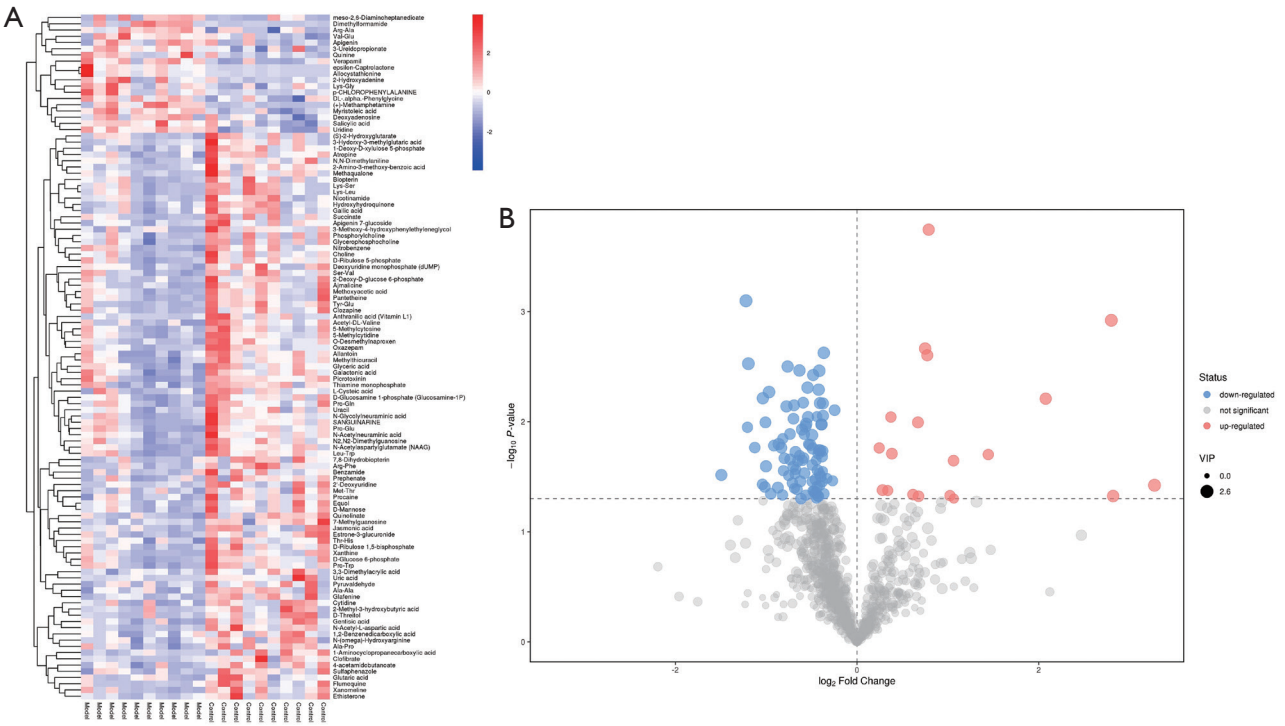

Figure 3 Comparison of all differentially expressed metabolites levels in the ketamine and control groups. Heatmaps showed 118 significantly altered metabolites between these two groups (A). The colors correspond to the abundance value of each metabolite. Volcano map showed differentially expressed metabolites screened by VIP value >1 and P<0.05 (B). VIP, variable importance in the projection.

than 1. There were 118 differential metabolites identified according to the qualitative matching analysis of the secondary MS (Table S1). Heatmaps and volcano maps were used to represent the screened differential metabolites (*Figure 3*). Out of the 118 differential metabolites, 16 were up-regulated and 102 were down-regulated (*Table 1*). The screened differential metabolites included myristoleic acid, L-homoserine, methamphetamine, dimethylformamide, anthranilic acid (vitamin L1), and others (*Table 1*).

Also, receiver operating characteristic (ROC) curves and box plots were used to find differential metabolites that were correlated with fibrosis trends. A total of 9 metabolites were identified with an area under the curve of ROC (AUC) greater than 0.9 (*Figure 4*). These differential expressed metabolites may be potential biomarkers in a rat model of ketamine induced bladder fibrosis.

Bioinformatics analysis of the differential expressed metabolites

The degree of correlation was measured by the correlation coefficient r, with positive correlations ranging from 0 to 1 and negative correlations ranging from 0 to –1. When the absolute value of r is closer to 1, a stronger correlation of the different metabolites is indicated. The results are presented as heatmaps (*Figure 5A*). To explore the relationship between metabolites and regulatory networks, metabolites were located based on KEGG database with relative metabolic responses, metabolic pathways and regulatory proteins. (*Figure 5B,C*). Based on the KEGG database, networks describing the metabolic and physiological processes were shown in *Figure 5D,E*. The enriched pathway included biosynthesis of amino acids, pyrimidine metabolism, and more (*Table 2*).

Discussion

In this study, a rat model of ketamine induced bladder damage and fibrosis was established by tail vein injection of ketamine. The model was confirmed by HE and Masson trichrome staining. Also, this report investigated the differential expression of urinary metabolites based on a metabolomic

Table 1 Partial results of differential metabolites in ketamine treated rat urine samples compared to control group

Metabolites	VIP	Fold change
Hydroxyphenyllactic acid	2.63	17.03
Epsilon-caprolactone	2.48	9.59
Allocystathionine	2.17	7.02
(+)-Methamphetamine	2.35	6.95
Dimethylformamide	1.94	4.21
Myristoleic acid	2.10	1.73
L-homoserine	1.75	1.55
Estrone-3-glucuronide	2.10	0.49
1-aminocyclopropanecarboxylic acid	1.79	0.46
N-acetyl-L-aspartic acid	2.40	0.44
Tyr-Glu	2.12	0.43
anthranilic acid (vitamin L1)	1.85	0.36

VIP, variable importance in the projection.

approach. A total of 118 differential expressed metabolites in urine samples were detected through metabolomic methods. Among them, hydroxyphenyllactic acid, epsilon-caprolactone, allocystathionine, methamphetamine, dimethylformamide, etc., were expressed differently, and the highest fold change reached to as high as 17. Myristoleic acid has been reported to induce apoptotic necrosis of prostate cells (16), L-homoserine may be involved in the induction of regulatory T cells (17), and dimethylformamide has been showed to be directly toxic to the kidneys (18). Some studies have been reported that the metabolites in urine may infiltrate into bladder urothelium, related to bladder damage (19). These results suggest that ketamine-induced bladder fibrosis may be related to its direct damage or metabolites, and immunomodulation. may be a potential pathogenesis. Also, methamphetamine, one of the differential metabolites in the ketamine-treated rats, has been reported to be involved in the urinary system's impairment. These urinary metabolites should be considered when analyzing the mechanisms of ketamine-associated urinary dysfunction (20,21).

There is currently no standardized method for establishing a rat model of ketamine induced urinary dysfunction, according to current literature the treatment concentrations were ranging from 5 to 60 mg/kg and treatment duration was ranging from 2 weeks to 4 months (9,22,23). In this study, animal model was established through tail vein injection of ketamine at 25 mg/kg for 8 consecutive weeks. Histopathological staining demonstrated bladder urothelial denudation, inflammatory cells infiltration, vasodilatation and extensive ECM deposition in the submucosa layer and between the detrusor muscle bundles, which indicated bladder inflammation and fibrosis. However, during 8 weeks of ketamine treatment, some rats were comatose or even died after ketamine rapid injection, which could be due to the quick increase of blood ketamine concentration through intravenous injection. In the further study, different treatment methods and duration should be explored to develop improved animal model protocol or guideline.

Based on bioinformatics analysis, differential metabolites are enriched in pathways such as pyrimidine metabolism, amino sugar and nucleotide sugar metabolism, ATP-binding cassette (ABC) transporters, phenylalanine, tyrosine and tryptophan biosynthesis and biosynthesis of amino acids. Previous research highlighted that KRP-103 in pyrimidine metabolism is associated with bladder dysfunction (24). In distention-induced rhythmic bladder contractions (RBCs) in urethane-anesthetized guinea pigs, KRP-103 injected by intravenous dose-dependently increased the shutdown time of RBCs and decreased the amplitude of RBCs (24). Bicyclic pyrimidine derivatives may be a candidate therapeutic drug for the treatment of overactive bladder (24). Another study also indicated a correlation between phenylalanine and liver fibrosis (25). Combining metabolic pathways may provide novel ideas for studying bladder dysfunction

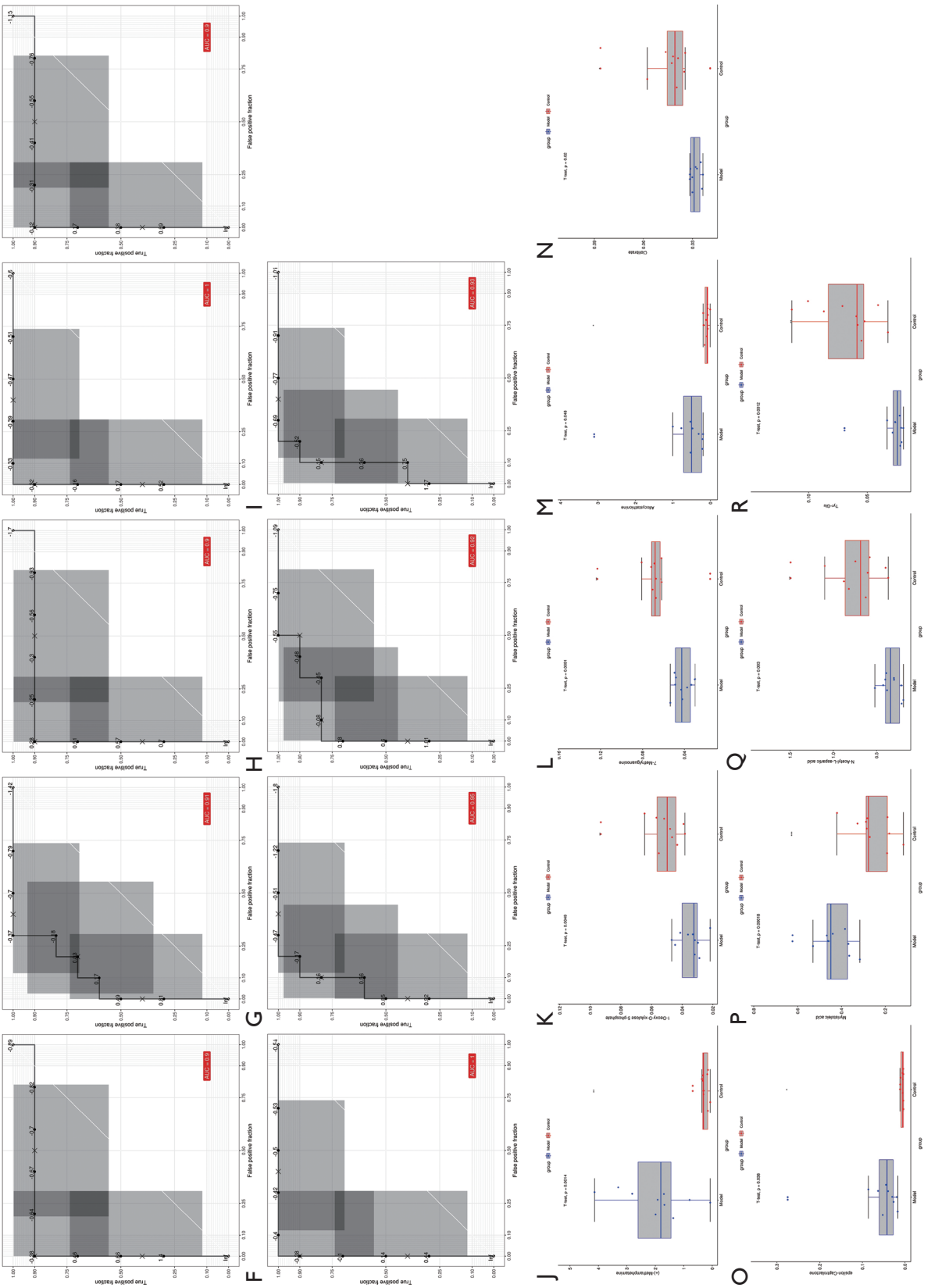

Figure 4 ROC curves (A,B,C,D,E,F,G,H,I,J) and box plots (K,L,M,N,O,P,Q,R) for differential metabolites screened with AUC >0.9. (A,J) Methamphetamine; (B,K) 1-deoxy-D-xylulose-5-phosphate; (C,L) 7-methylguanosine; (D,M) allocystathionine; (E,N) clofibrate; (F,O) epsilon-caprolactone; (G,P) myristoleic acid; (H,Q) N-acetyl-L-aspartic acid; (I,R) Tyr-Glu. AUC, area under the curve of ROC.

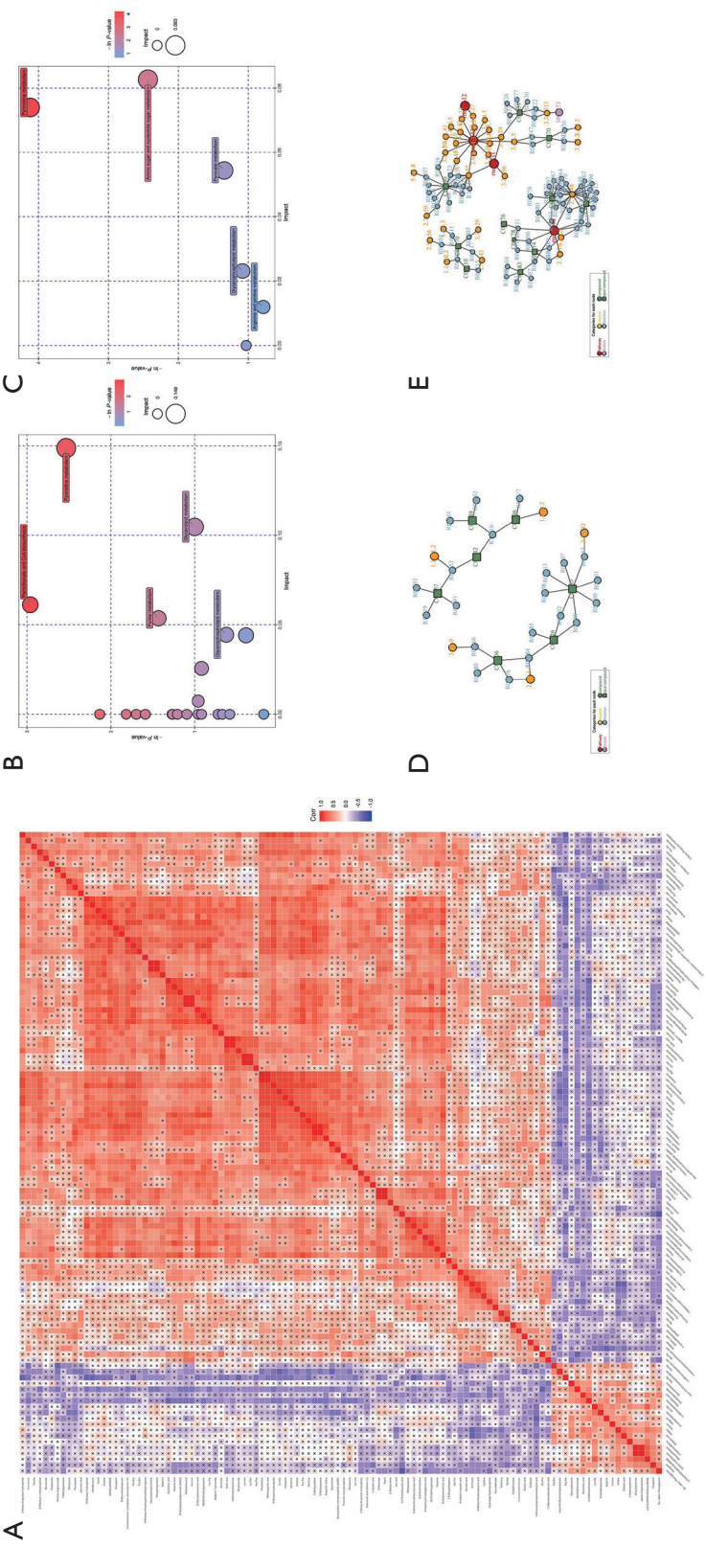

Figure 5 Heatmap of correlation analysis for differential metabolites (A). Pathway analysis bubble plot for model group *vs.* control group (B for negative ion and C for positive ion mode). Regulatory network map for model group vs. control group (D for negative ion and E for positive ion mode).

Table 2 Partial enriched pathway of differential metabolites

Pathway ID in KEGG database	Description of pathway	Compounds number
rno01100	Metabolic pathways	46
rno00240	Pyrimidine metabolism	8
rno00520	Amino sugar and nucleotide sugar metabolism	6
rno01230	Biosynthesis of amino acids	5
rno00400	Phenylalanine, tyrosine and tryptophan biosynthesis	4

and fibrosis. Further studies of metabolites, including targeted metabolomics studies, may generate meaningful information regarding signal pathways and pathogenesis.

Currently, ketamine-induced cystitis diagnosis mainly relies on a history of ketamine abuse and clinical symptoms as assessed by a urologist. Differential diagnosis can be hampered by patients not being upfront about their drug abuse history or if clinical symptoms are missed. To date, no urine biomarkers have been developed for the clinical detection of bladder dysfunction and fibrosis. Early diagnosis in patients with bladder fibrosis is one of the key factors in improving clinical outcomes. Some reports have already provided evidences about the application of urine metabolites in urinary diseases, such as interstitial cystitis, chronic prostatitis, bladder cancer and other urological disorders (26-28). In the ROC curves, metabolites with a large AUC values were identified as promising potential biomarkers for the ketamine-induced bladder rat model. These urinary metabolites may be potential biomarker in the clinical diagnosis of ketamine induced bladder dysfunction and the early detection of bladder fibrosis, and further research in animal models and ketamine abusers are warranted.

Conclusions

A rat model of ketamine-induced bladder fibrosis was successfully established. The expressions of urine metabolites in this model were analyzed through metabolomic method. A total of 118 differential metabolites were detected, 16 of which were up-regulated and 102 were down-regulated. Combined with bioinformatics approaches, the biological functions of the differential urine metabolites were analyzed. Related pathways included pyrimidine metabolism, amino sugar, phenylalanine, tyrosine and tryptophan biosynthesis, etc. It provided vital clues for understanding the pathogenesis, and further aids in the diagnosis and treatment of ketamine-induced bladder dysfunction and fibrosis.

Acknowledgments

The authors are grateful to Biotree Biotech (Co., Ltd., Shanghai, China) for technical support.

Funding: This work was supported by the National Natural Science Foundation of China (grant No. 81700667).

Footnote

Reporting Checklist: The authors have completed the ARRIVE reporting checklist. Available at http://dx.doi.org/10.21037/tau-20-1202

Data Sharing Statement: Available at http://dx.doi.org/10.21037/tau-20-1202

Conflicts of Interest: All authors have completed the ICMJE uniform disclosure form (available at http://dx.doi.org/10.21037/tau-20-1202). The authors have no conflicts of interest to declare.

Ethical Statement: The authors are accountable for all aspects of the work in ensuring that questions related to the accuracy or integrity of any part of the work are appropriately investigated and resolved. Experiments were performed under a project license (No. 2018sydw0225) granted by experimental animal welfare center in Central South University, Hunan, China, in compliance with China's "Animal management regulations" for the care and use of animals.

References

1. Bokor G, Anderson P. Ketamine: an update on its abuse. J Pharm Pract 2014;27:582-6.
2. Trujillo KA, Smith ML, Sullivan B, et al. The neurobehavioral pharmacology of ketamine: implications for drug abuse, addiction, and psychiatric disorders. ILAR J 2011;52:366-78.
3. Shahani R, Streutker C, Dickson B, et al. Ketamine-associated ulcerative cystitis: a new clinical entity. Urology 2007;69:810-2.
4. Chung SD, Wang CC, Kuo HC. Augmentation enterocystoplasty is effective in relieving refractory ketamine-related bladder pain. Neurourol Urodyn 2014;33:1207-11.
5. Hopcroft SA, Cottrell AM, Mason K, et al. Ureteric intestinal metaplasia in association with chronic recreational ketamine abuse. J Clin Pathol 2011;64:551-2.
6. Peng TR, Lee MC, Wu TW, et al. Suspected ketamine-associated lower urinary tract symptoms. Urol J 2014;11:1508-10.
7. Castellani D, Pirola G, Gubbiotti M, et al. What urologists need to know about ketamine-induced uropathy: A systematic review. Neurourol Urodyn 2020;39:1049-62.
8. Ou YL, Liu CY, Cha TL, et al. Complete reversal of the clinical symptoms and image morphology of ketamine cystitis after intravesical hyaluronic acid instillation: A case report. Medicine (Baltimore) 2018;97:e11500.
9. Wang J, Chen Y, Gu D, et al. Ketamine-induced bladder fibrosis involves epithelial-to-mesenchymal transition mediated by transforming growth factor-β1. Am J Physiol Renal Physiol 2017;313:F961-72. Erratum in: Am J Physiol Renal Physiol. 2018 Feb 1;314(2):F317. doi: 10.1152/ajprenal.zh2-8423-corr.2017.
10. Wu P, Wang Q, Huang Z, et al. Clinical staging of ketamine-associated urinary dysfunction: a strategy for assessment and treatment. World J Urol 2016;34:1329-36.
11. Jhang JF, Hsu YH, Kuo HC. Possible pathophysiology of ketamine-related cystitis and associated treatment strategies. Int J Urol 2015;22:816-25.
12. Hiller K, Hangebrauk J, Jäger C, et al. MetaboliteDetector: comprehensive analysis tool for targeted and nontargeted GC/MS based metabolome analysis. Anal Chem 2009;81:3429-39.
13. Evans AM, DeHaven CD, Barrett T, et al. Integrated, nontargeted ultrahigh performance liquid chromatography/electrospray ionization tandem mass spectrometry platform for the identification and relative quantification of the small-molecule complement of biological systems. Anal Chem 2009;81:6656-67.
14. Fischer AH, Jacobson KA, Rose J, et al. Hematoxylin and eosin staining of tissue and cell sections. CSH Protoc 2008;2008:pdb.prot4986.
15. Ozawa A, Sakaue M. New decolorization method produces more information from tissue sections stained with hematoxylin and eosin stain and masson-trichrome stain. Ann Anat 2020;227:151431.
16. Iguchi K, Okumura N, Usui S, et al. Myristoleic acid, a cytotoxic component in the extract from Serenoa repens, induces apoptosis and necrosis in human prostatic LNCaP cells. Prostate 2001;47:59-65.
17. Li Y, Zhou H, Zhang Y, et al. N-3-(oxododecanoyl)-L-homoserine lactone promotes the induction of regulatory T-cells by preventing human dendritic cell maturation. Exp Biol Med (Maywood) 2015;240:896-903.
18. Hu ZY, Chang J, Guo FF, et al. The effects of dimethylformamide exposure on liver and kidney function in the elderly population: A cross-sectional study. Medicine (Baltimore) 2020;99:e20749.
19. Moraes JP, Pereira DS, Matos AS, et al. The ethanol extract of the inner bark of Caesalpinia pyramidalis (Tul.) reduces urinary bladder damage during cyclophosphamide-induced cystitis in rats. ScientificWorldJournal 2013;2013:694010.
20. Bennett AH, Delrio A. Idiopathic rupture of the bladder: association with methamphetamine and alcohol. J Urol 1980;124:429-30.
21. Delgado JH, Caruso MJ, Waksman JC, et al. Acute, transient urinary retention from combined ecstasy and methamphetamine use. J Emerg Med 2004;26:173-5.
22. Cui L, Jiang X, Zhang C, et al. Ketamine induces endoplasmic reticulum stress in rats and SV-HUC-1 human uroepithelial cells by activating NLRP3/TXNIP aix. Biosci Rep 2019;39:BSR20190595.
23. Kim A, Yu H, Heo J, et al. Mesenchymal stem cells protect against the tissue fibrosis of ketamine-induced cystitis in rat bladder. Sci Rep 2016;6:30881.
24. Tanioka A, Deguchi T. Effect of a Bicyclic Pyrimidine Derivative (KRP-103), a Novel Selective Tachykinin NK1 Receptor Antagonist, on Bladder Function in Guinea Pigs.

Drug Res (Stuttg) 2017;67:302-7.
25. Wada M, Wada Y, Uchiyama M, et al. (13)C-phenylalanine breath test correlates with liver fibrosis in postoperative biliary atresia. Pediatr Int 2007;49:836-41.
26. Kind T, Cho E, Park T, et al. Interstitial Cystitis-Associated Urinary Metabolites Identified by Mass-Spectrometry Based Metabolomics Analysis. Sci Rep 2016;6:39227.
27. Shoskes DA, Altemus J, Polackwich AS, et al. The Urinary Microbiome Differs Significantly Between Patients With Chronic Prostatitis/Chronic Pelvic Pain Syndrome and Controls as Well as Between Patients With Different Clinical Phenotypes. Urology 2016;92:26-32.
28. Witzke KE, Großerueschkamp F, Jütte H, et al. Integrated Fourier Transform Infrared Imaging and Proteomics for Identification of a Candidate Histochemical Biomarker in Bladder Cancer. Am J Pathol 2019;189:619-31.

Cite this article as: Li H, Zhu Q, Li K, Wu Z, Tang Z, Wang Z. Investigation of urinary components in rat model of ketamine-induced bladder fibrosis based on metabolomics. Transl Androl Urol 2021;10(2):830-840. doi: 10.21037/tau-20-1202

Supplementary

Table S1 All differential metabolites in ketamine treated rat urine samples compared to control group

MS2 name	Type	VIP	P value	Fold change
p-Chlorophenylalanine	MS2 reverse	1.482664661	0.022581683	2.088403489
Myristoleic acid	MS2 reverse	2.09799238	0.000179994	1.726790289
Salicylic acid	MS2 forward	1.824331269	0.010147158	1.591570624
L-homoserine	MS2 reverse	1.746636855	0.010277906	1.548048138
3-Methoxy-4-hydroxyphenylethyleneglycol	MS2 reverse	1.370359686	0.034436936	0.829686969
Sulfaphenazole	MS2 reverse	1.029843202	0.03273948	0.795389004
1,2-Benzenedicarboxylic acid	MS2 forward	1.5430191	0.045110528	0.777020585
Quinolinate	MS2 forward	2.082448204	0.00236724	0.775982736
D-glucosamine 1-phosphate	MS2 forward	1.833854214	0.008842721	0.771064659
Phosphorylcholine	MS2 forward	1.117232921	0.028263596	0.769568172
D-ribulose 5-phosphate	MS2 forward	1.780321548	0.018475696	0.768976317
Allantoin	MS2 forward	2.046300074	0.010595984	0.762709318
Glyceric acid	MS2 reverse	2.121688111	0.01057002	0.761944433
Galactonic acid	MS2 forward	1.951851055	0.0313966	0.758280251
Picrotoxinin	MS2 reverse	2.079133994	0.018233279	0.755109009
Thiamine monophosphate	MS2 reverse	2.063228119	0.006774628	0.75347008
N-Acetylaspartylglutamate (NAAG)	MS2 reverse	2.291827297	0.003445462	0.749532403
Methylthiouracil	MS2 reverse	2.160625989	0.005118714	0.746049357
Glutaric acid	MS2 reverse	1.557278238	0.047708268	0.745016803
L-Cysteic acid	MS2 reverse	1.623170822	0.04716071	0.741823206
3',5'-Cyclic guanosine monophosphate	MS2 forward	1.710857486	0.020098057	0.730690388
N-Acetylneuraminic acid	MS2 forward	1.749960452	0.033525987	0.728765601
Biopterin	MS2 forward	1.227077427	0.044781799	0.722976261
Hydroxyproline	MS2 reverse	1.901941039	0.031785026	0.719187455
(S)-2-Hydroxyglutarate	MS2 forward	1.610349719	0.034992987	0.710700459
D-Glucose 6-phosphate	MS2 reverse	2.086381705	0.004901267	0.685505863
3-Hydorxy-3-methylglutaric acid	MS2 forward	1.501667044	0.046499813	0.67649715
Xanthine	MS2 forward	2.091674633	0.011043818	0.674563903
Gallic acid	MS2 forward	1.468370852	0.01298651	0.669149235
Succinate	MS2 forward	1.649946217	0.021349092	0.665581289
Uracil	MS2 forward	1.52020403	0.022438883	0.659230513
3-Hydroxyisovaleric acid	MS2 reverse	1.667482832	0.021694764	0.647310844
Allocystathionine	MS2 reverse	1.883617934	0.038591377	0.646847067
2'-Deoxyuridine	MS2 reverse	1.230308737	0.040283808	0.620371895
Hydroxyhydroquinone	MS2 reverse	1.662096942	0.007088873	0.618218772
Deoxyuridine monophosphate	MS2 reverse	1.649252621	0.025565738	0.614569781
Jasmonic acid	MS2 reverse	1.514285312	0.036044238	0.610840674
Pantetheine	MS2 forward	1.675574703	0.022016291	0.600185386
Apigenin 7-glucoside	MS2 reverse	1.580735469	0.021473258	0.574226734
Prephenate	MS2 reverse	1.358369196	0.014242113	0.567506361
2-Amino-3-methoxy-benzoic acid	MS2 reverse	1.787397399	0.017242521	0.561417149
5-Hydroxymethylcytidine	MS2 reverse	1.396897031	0.019620982	0.556911219
L-Ascorbic acid	MS2 forward	1.413277202	0.048514968	0.5558384
D-Ribulose 1,5-bisphosphate	MS2 reverse	2.031981268	0.015979171	0.550204342
Oxazepam	MS2 reverse	1.860735515	0.039675759	0.54668473
L-Histidinol	MS2 reverse	1.613477995	0.021146814	0.53101848
D-Threitol	MS2 forward	1.902102624	0.016490356	0.530728427
Uric acid	MS2 forward	1.720076229	0.045187868	0.517918642
Glafenine	MS2 reverse	2.137081115	0.005373777	0.5110753
Clozapine	MS2 reverse	1.939712787	0.025412069	0.499340036
2-Deoxy-D-glucose 6-phosphate	MS2 reverse	1.656468689	0.039200661	0.495137978
Estrone-3-glucuronide	MS2 reverse	2.097005256	0.006118495	0.487421812
2-Methyl-3-hydroxybutyric acid	MS2 reverse	1.72070876	0.037063118	0.486247008
N-Acetyl-L-aspartic acid	MS2 reverse	2.398347827	0.002969733	0.436451439
Anthranilic acid (Vitamin L1)	MS2 reverse	1.858261397	0.030461366	0.355221406
Hydroxyphenyllactic acid	MS2 reverse	2.633650228	0.019664464	17.03006355
Epsilon-caprolactone	MS2 reverse	2.477916359	0.038380883	9.592274572
Allocystathionine	MS2 reverse	2.172458016	0.0480407	7.017815453

Table S1 (*continued*)

http://dx.doi.org/10.21037/tau-20-1202

Table S1 (*continued*)

MS2 name	Type	VIP	P value	Fold change
(+)-Methamphetamine	MS2 forward	2.347313599	0.001415391	6.949027624
Dimethylformamide	MS2 reverse	1.940048907	0.006059808	4.206489916
Meso-2,6-diaminoheptanedioate	MS2 reverse	1.257826352	0.023069712	2.675236496
Uridine	MS2 reverse	2.020893568	0.003712476	1.699312722
Verapamil	MS2 reverse	2.16242187	0.002288484	1.683733074
Lys-Gly	MS2 reverse	1.473315216	0.0448077	1.520242251
Arg-Ala	MS2 reverse	1.377219343	0.0099348	1.301056568
Val-Glu	MS2 reverse	1.718494154	0.025726621	1.2977372
DL-alpha-phenylglycine	MS2 reverse	1.694713395	0.014759062	1.183587801
4-acetamidobutanoate	MS2 forward	1.624612075	0.008246869	0.843757376
O-Desmethylnaproxen	MS2 reverse	1.520776335	0.005264959	0.769378923
5-Methylcytosine	MS2 forward	1.64652063	0.013511683	0.76512237
Thymidine	MS2 reverse	1.496465311	0.017604915	0.761783666
Acetylglycine	MS2 reverse	1.255082407	0.020875357	0.759055512
Pro-Glu	MS2 forward	1.476630987	0.033605868	0.75816417
Thr-His	MS2 reverse	1.220499196	0.036751716	0.751130341
5-Methylcytidine	MS2 forward	1.658484074	0.014583692	0.745343053
Nitrobenzene	MS2 reverse	1.209341788	0.03705139	0.744022402
3,3-Dimethylacrylic acid	MS2 forward	1.589224968	0.02691495	0.740013662
Ser-Val	MS2 reverse	1.555183809	0.024983138	0.738083133
N-(omega)-Hydroxyarginine	MS2 reverse	1.333257353	0.009896441	0.730639649
Glycerophosphocholine	MS2 forward	1.078812605	0.018463782	0.729971001
Sanguinarine	MS2 reverse	1.494057237	0.043342222	0.723800293
Anthranilic acid (vitamin L1)	MS2 reverse	1.163473953	0.02848806	0.717913533
Atropine	MS2 reverse	1.679877549	0.004653833	0.712118058
N2,N2-Dimethylguanosine	MS2 reverse	1.755659554	0.01585386	0.7087619
N-Acetyl-D-glucosamine	MS2 forward	1.629226838	0.01782848	0.707239534
Biopterin	MS2 forward	1.000834999	0.042091843	0.705518001
Pro-Trp	MS2 reverse	1.793857835	0.014064219	0.704400066
Cytidine	MS2 reverse	1.574311055	0.018826082	0.703354023
Flumequine	MS2 reverse	1.813932221	0.010658893	0.703252572
Pyruvaldehyde	MS2 reverse	1.142383824	0.049498601	0.700527032
Met-Thr	MS2 reverse	1.249302443	0.021575958	0.694715977
Leu-Trp	MS2 reverse	1.745869501	0.00711319	0.682205215
Xanomeline	MS2 reverse	1.923823003	0.008476593	0.674795605
Ala-Pro	MS2 reverse	1.579299618	0.005411376	0.661127047
N-Glycolylneuraminic acid	MS2 reverse	1.57156514	0.030426096	0.659859161
Acetyl-DL-Valine	MS2 reverse	1.734203519	0.011445194	0.655074708
Ethisterone	MS2 reverse	1.755203974	0.032942997	0.649340674
1-Deoxy-D-xylulose 5-phosphate	MS2 reverse	1.893722005	0.004923546	0.643672651
Clofibrate	MS2 reverse	1.778152384	0.019533896	0.639236238
N-Acetylneuraminic acid	MS2 forward	1.893214103	0.011852953	0.637754926
Procaine	MS2 reverse	1.267212456	0.021033961	0.634484755
Methoxyacetic acid	MS2 reverse	1.613501592	0.017177443	0.62354792
N,N-Dimethylaniline	MS2 reverse	1.38670469	0.047154221	0.622392371
Lys-Leu	MS2 reverse	1.226355959	0.026133676	0.621554911
Lys-Ser	MS2 reverse	1.248923791	0.027392882	0.619395745
Ala-Ala	MS2 reverse	1.563839603	0.00849707	0.606806261
7-Methylguanosine	MS2 reverse	1.712194102	0.009144798	0.603191597
Equol	MS2 forward	1.255913117	0.030707226	0.588731875
Malonic acid	MS2 reverse	1.965097321	0.004436536	0.583918122
Ajmalicine	MS2 reverse	1.687588952	0.007489708	0.582624244
D-Mannose	MS2 forward	1.286248655	0.033116293	0.563901819
Quinate	MS2 reverse	1.422653095	0.039765564	0.559847402
Arg-Phe	MS2 forward	1.665346043	0.010164035	0.493562524
1-Aminocyclopropanecarboxylic acid	MS2 reverse	1.78917087	0.017018907	0.458740484
7,8-Dihydrobiopterin	MS2 forward	1.424846621	0.010708745	0.430668925
Tyr-Glu	MS2 reverse	2.119367582	0.00081498	0.428884596

http://dx.doi.org/10.21037/tau-20-1202